TECHNICAL NOTE

Revisiting the Evaluation of Hydraulic Transmissivity of Elliptical Rock Fractures in Triaxial Shear-Flow Experiments

Yinlin Ji[1,2] · Hannes Hofmann[1] · Ernest H. Rutter[3] · Fei Xiao[4] · Lining Yang[3]

Highlights
- A novel numerical approach has been proposed to retrieve the hydraulic transmissivity of elliptical rock fractures in triaxial shear-flow experiments.
- The accuracy of different methods for estimation of hydraulic transmissivity of elliptical rock fractures has been evaluated and discussed.
- The numerical approach and electrical analogy are recommended for accurate evaluation of hydraulic transmissivity of elliptical rock fractures.

List of Symbols

Ψ	Fracture inclination angle with respect to the sample axis
$2a$	Length along slip-parallel direction
$2b$	Length along slip-normal direction
B	Geometry constant
d	Distance between borehole and ellipse edge
k	Permeability
L	Length along the flow direction
n	Ratio between b and a
q	Fluid flux
Q	Volumetric flow rate
Q_{exp}	Volumetric flow rate recorded in the laboratory
r	Borehole radius
t	Effective thickness of fracture
w	Fracture width
Δp	Pressure difference between the inlet and outlet boreholes
μ	Dynamic viscosity of fluid
∇p	Pressure drop over a given distance

✉ Yinlin Ji
  yinlinji@gfz-potsdam.de

✉ Fei Xiao
  fei.xiao@nuaa.edu.cn

1 Helmholtz Centre Potsdam GFZ German Research Centre for Geosciences, 14473 Potsdam, Germany

2 State Key Laboratory of Coal Resources and Safe Mining, China University of Mining and Technology, Xuzhou 221116, Jiangsu, China

3 Rock Deformation Laboratory, Department of Earth and Environmental Sciences, The University of Manchester, Manchester M139PL, UK

4 Department of Civil Engineering, College of Aerospace Engineering, Nanjing University of Aeronautics and Astronautics, Nanjing 210016, China

1 Introduction

Understanding the evolution of hydraulic transmissivity of rock fractures under various hydromechanical conditions is vital to the successful exploitation of geo-energy systems (e.g., Bossart et al. 2002; Ellsworth 2013; Fang et al. 2017; Im et al. 2018; Ji et al. 2019, 2020, 2021, 2022; LongJohn et al. 2018; Ma and Zoback 2017; Passelègue et al. 2018; Shovkun and Espinoza 2017; Shapiro et al. 1997; Shen et al. 2020; Zoback 2010). The hydraulic transmissivity of a rock fracture is defined as the product of the permeability of the material within the fracture with the effective thickness of the fracture, and has a dimension of m[3] (Acosta et al. 2020; Passelègue et al. 2020; Rutter and Mecklenburgh 2017, 2018). Considerable experimental effort has been made to investigate the hydromechanical properties of rock fractures. In these studies using different experimental setups, the triaxial shear-flow setup has three major advantages over the

other configurations, including the direct shear-flow setup, double direct shear-flow setup, and rotary shear-flow setup (Ji et al. 2021). First, it can be readily deployed in conventional triaxial cells equipped with fluid pumps. Second, the good sealing provided by the jacket material allows for the easier and safer application of relatively high fluid pressures within pores and fractures, which can almost reach but be slightly lower than the confining pressure (e.g., Ji 2020; Ye and Ghassemi 2018; Wang et al. 2020). Third, the hydraulic properties of rock fractures can be evaluated in different directions (i.e., parallel or normal to the slip direction) while the fracture is subjected to mechanical loading (Okazaki et al. 2013; Rutter and Mecklenburgh 2017, 2018). In triaxial shear-flow experiments, an inclined fracture is prepared in a cylindrical rock sample and the fluid gains access to and egress from the fracture normally through small boreholes made to intersect the fracture plane (Ji et al. 2021). However, the rock fracture in triaxial shear-flow experiments on samples fabricated from cylindrical cores is an ellipse with an unknown effective thickness and a variable fracture width along the flow path, posing difficulties for the evaluation of its hydraulic transmissivity. The transmissivity of a rock fracture with a constant fracture width can be estimated based on Darcy's law (Acosta et al. 2020). Thus, a rectangular approximation, in which a constant fracture width is assumed, has been proposed to provide an estimation of the transmissivity of a rock fracture that is elliptical in shape (e.g., Crawford et al. 2008; Jeppson et al. 2021; Bijay and Ghazanfari 2021; Okazaki et al. 2013; Wang et al. 2021; Ye and Ghassemi 2018). However, the transmissivity of an elliptical rock fracture can also be derived analytically based on the electrical analogy with the flow of electric current in a planar sheet of elliptical shape (Rutter and Mecklenburgh 2017, 2018), so that it is no longer necessary to use a rectangular approximation (Acosta et al. 2020; Passelègue et al. 2020). Nevertheless, given the extensive use of the rectangular approximation and electrical analogy, the relative accuracy of the rectangular approximation and the electrical analogy should be evaluated and discussed for better interpretation and comparison of inter-laboratory results.

In the laboratory, the hydraulic properties of a sample with a relatively large transmissivity can be measured by the steady state flow method (Scheidegger 1958), which records the volumetric flow rate of fluid through the sample under a constant fluid pressure difference between the two sample ends. However, the steady state flow measurements can become too time-consuming for very low transmissivity samples (Milsch et al. 2016). In such cases transmissivity can be measured by transient flow methods, such as the pulse decay method (Brace et al. 1968) and the oscillating pressure method (Kranz et al. 1990; Fischer 1992; Faulkner and Rutter 2000; Bernabe et al. 2006). In either steady state flow or transient flow measurements of fracture transmissivity, the flow boundary shape is an important factor that substantially influences the accuracy of transmissivity evaluation.

The objective of this study is to revisit the evaluation of hydraulic transmissivity of elliptical rock fractures in triaxial shear-flow experiments. The significance of this study lies in the proposal of a novel numerical back-calculation method for determining the transmissivity of an elliptical rock fracture, the accuracy evaluation of the two commonly used transmissivity estimation methods, and the final recommendations.

2 Triaxial Shear-Flow Experiments

2.1 Experimental Configuration

Triaxial shear-flow experiments are readily performed in conventional triaxial cells, which can apply axial stress and confining pressure independently. The loading path of shear and normal stresses on the fracture inclined at an angle Ψ (°) to the sample axis can be adjusted by servocontrol of the axial stress and confining pressure (Fig. 1). Particularly, the confining pressure is updated continuously under computer control during the experiments to maintain a constant normal stress on the fracture, taking into account the contact area reduction and jacket deformation with shear displacement (Ji 2020, Sect. 3.3; Tembe et al. 2010, Appendix A). The inclined fracture can be a smooth sawcut fracture (e.g., Ji et al. 2021; Rutter and Mecklenburgh 2017, 2018), a rough tensile or natural fracture (e.g., Byerlee 1967; Ji and Wu et al. 2020), or may be filled with granular powders with various particle sizes and mineral components (e.g., Marone and Scholz 1989; Tembe et al. 2010).

For most rocks, the rate of increase of strength with confining pressure leads to a fresh fault forming at around $\Psi = 25°$–30° to the maximum compressive stress direction (Sibson 1990). In triaxial shear-flow experiments that employ a pre-cut 'fracture', it is not essential to use this 'optimal' inclination angle for Ψ. The only constraint is that Ψ should lie within the range of about 20°–55°, depending on the magnitude of the cohesive strength, to avoid the formation of a fresh fault in the rock matrix at the 'optimal' angle (Brady and Brown 1993). In previous studies using the triaxial shear-flow configuration the most frequently used pre-cut fracture inclination angles have been 30° (e.g., Ji, 2020; Passelègue et al. 2018) and 45° (e.g., Rutter and Mecklenburgh 2017, 2018).

The transmissivity of the rock matrix in relation to the fracture transmissivity is another major consideration. The rock matrix transmissivity should be low enough to be negligible compared to the fracture transmissivity during the experiments, thus confining the fluid flow within the relatively conductive fracture plane (Ji et al. 2021). To evaluate

Fig. 1 Triaxial shear-flow setup with an elliptical rock fracture inclined at Ψ to the sample axis. The axial stress and confining pressure on the sample (left) can be resolved as the shear and normal stresses on the fracture (middle). Two boreholes are drilled near the edges as inlet and outlet boreholes to facilitate fluid communication with the rock fracture (right). **a** Transmissivity measurement along slip-parallel direction. **b** Transmissivity measurement along slip-normal direction
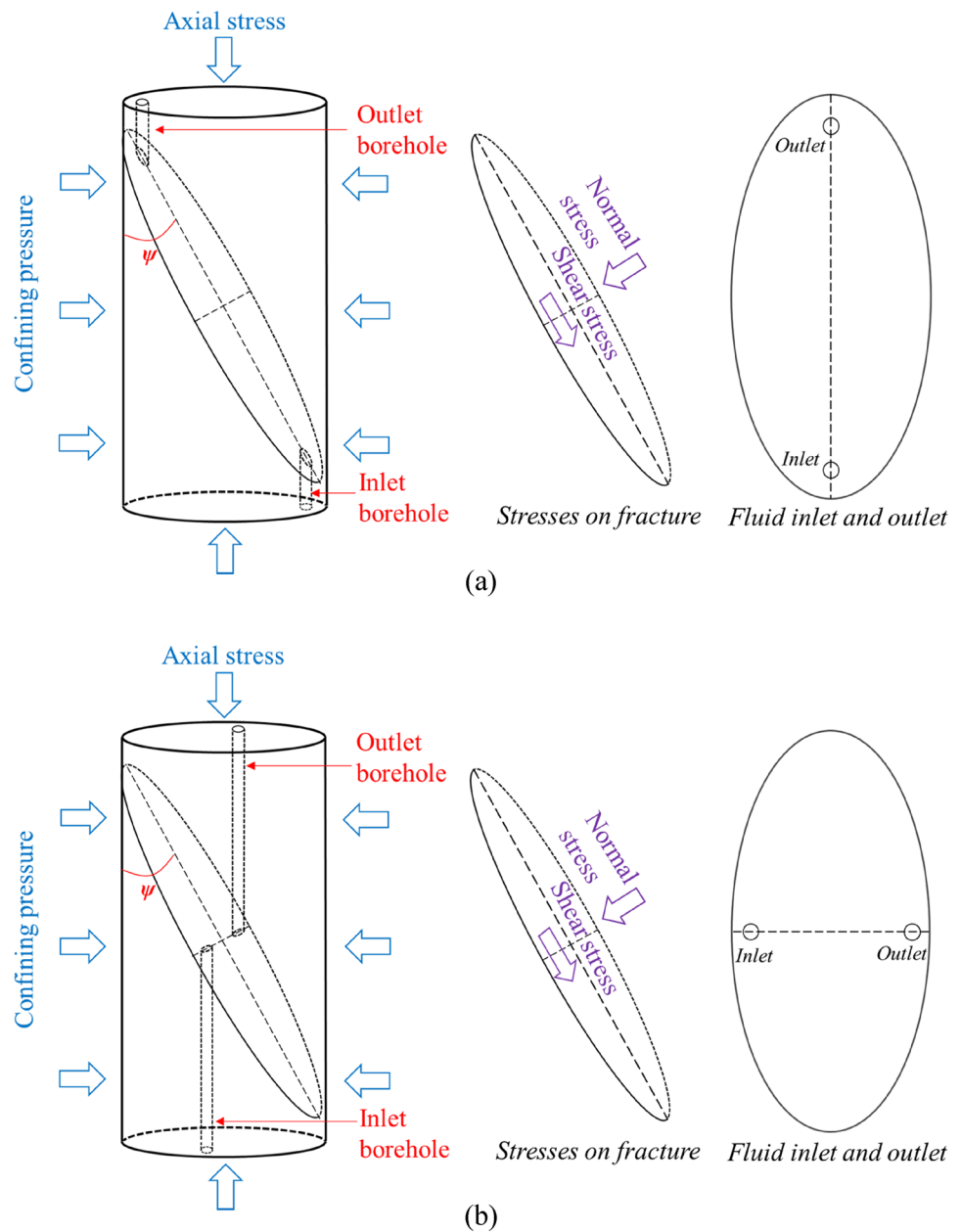
the hydraulic transmissivity of the rock fracture parallel to the slip direction, two boreholes (inlet and outlet) are drilled from the sample ends to intersect the major axis of the fracture near its ends (Fig. 1a). The slip-normal hydraulic transmissivity of the rock fracture can be measured by drilling two similar boreholes near the edges on the minor axis of the fracture (Fig. 1b).

2.2 Experimental Details

To illustrate the comparability between the numerical estimation of hydraulic transmissivity and the value obtained using the electrical analogy, we have used the steady state flow measurement data in the triaxial shear-flow experiments reported by Ye and Ghassemi (2018) as the source data, including the inlet and outlet pressures and volumetric flow rate. The purpose of their study was to investigate the slip-parallel transmissivity evolution of rock fractures with cumulative injection-induced shear displacement. Cylindrical samples with a diameter of 50 mm and a length of 100 mm were cored from the Sierra White granite. A fracture inclined 30° to the sample axis was prepared in the core sample. Two small boreholes were drilled near the edges on the major axis of the fracture to measure the slip-parallel hydraulic transmissivity (Fig. 1a). Distilled water was used as the pore fluid. Four fractures, including two

sawcut fractures and two tensile fractures, were used in their study. The JRC (joint surface roughness) values of the four fractures ranged from 1.19 to 15.32, which means the steady state flow measurement data was harvested from fractures with a wide range of surface roughnesses, considering the fact that the full range of JRC was from 0 to 20 (Barton 1973). On each rock fracture, a suite of tests was performed under a total confining pressure of 30 MPa and a near-critical shear stress under the constant axial displacement control. The inlet pressure was increased step-wise at a rate of 0.03 MPa/s from 5 to 28 MPa to induce fracture slip, and then decreased step-wise from 28 to 8 MPa at the same rate to check whether the hydraulic transmissivity was retained after the injection-induced shear slip. The outlet pressure was maintained constant at 5 MPa throughout the tests. At each inlet pressure step (i.e., 8, 12, 16, 20, 24, and 28 MPa), when the volumetric flow rate of the inlet pump was similar to that of the outlet pump (difference less than 5%), the fluid flow was considered to be steady state and the volumetric flow rate was recorded. More details of these tests and the raw data can be found in Ye and Ghassemi (2018).

3 Methods for Hydraulic Transmissivity Evaluation

Here we detail the three methods for hydraulic transmissivity evaluation, including the numerical back-calculation proposed in this study, the electrical analogy derived by Rutter and Mecklenburgh (2017, 2018), and the rectangular approximation used in e.g., Crawford et al. (2008), Jeppson et al. (2021), Bijay and Ghazanfari (2021), Okazaki et al. (2013), Wang et al. (2021), and Ye and Ghassemi (2018). In these three methods, the inlet and outlet fluid pressures as well as the volumetric flow rate measured directly using the steady state flow method in the laboratory are used for the transmissivity estimation based on Darcy's law. The numerical back-calculation and electrical analogy consider the exact elliptical shape of the fracture, while the third method makes a rectangular approximation to the elliptical fracture.

3.1 Numerical Back-Calculation

The COMSOL multi-physics software has been proved as a powerful finite element analysis tool for investigating fluid flow through rock fractures (e.g., Li et al. 2009; Ji et al., 2020; Wanniarachchi et al. 2018). In this study, we built a numerical model using the COMSOL multi-physics software to back-calculate the hydraulic transmissivity of the elliptical rock fracture based on the measured inlet and outlet pressures, volumetric flow rates and fracture geometry. The elliptical rock fracture (Fig. 2a, left) was simulated by an ellipse with the same major and minor axes as the elliptical

(a)

(b)
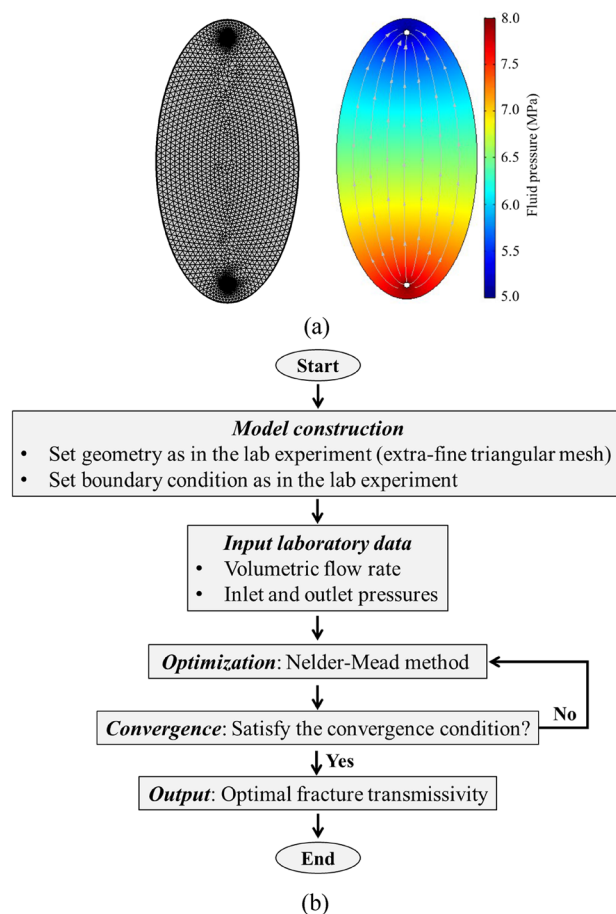
Fig. 2 Numerical back-calculation of hydraulic transmissivity of the elliptical rock fracture. **a** Left: Finite element model of the elliptical rock fracture with 100 mm major axis and 50 mm minor axis in the COMSOL multi-physics software with an extra-fine mesh. The boreholes with a radius of 1 mm are introduced on the major axis at 5 mm from the edge. Right: Example of steady state fluid pressure distribution with inlet and outlet pressures of 8 MPa and 5 MPa, respectively. The grey lines with arrows are the flow lines. **b** Flow chart showing the numerical back-calculation process of fracture transmissivity using the COMSOL multi-physics software

fracture. Two boreholes with a radius of r [mm] located at d [mm] from the respective edge on the major axis were introduced as the inlet and outlet boreholes. Fig. 2a (left) shows a numerical model of an elliptical rock fracture tested in Ye and Ghassemi (2018) with major and minor axes of 100 mm and 50 mm, respectively. The borehole radius r is 1 mm and the distance d between the borehole and the ellipse edge is 5 mm. The elliptical boundary is set as no-flow boundary. A highly accurate solution can be obtained by using an extra-fine triangular mesh with maximum and minimum element sizes of 2 and 0.0075 mm, respectively. We used Darcy's law to describe the fluid flow through the simulated fracture:

Fig. 3 Evaluation of the hydraulic transmissivity of an elliptical rock fracture using the electrical analogy (adapted from Rutter and Mecklenburgh 2018) and the rectangular approximation (adapted from Ye and Ghassemi 2018). 2*a* and 2*b* are the lengths along slip-parallel and slip-normal directions, respectively. *L* and *w* are the length and width of the assumed rectangular flow region (delineated by red dashed lines), respectively. *L* = 2*a* if the boreholes are assumed to lie on the elliptical boundary
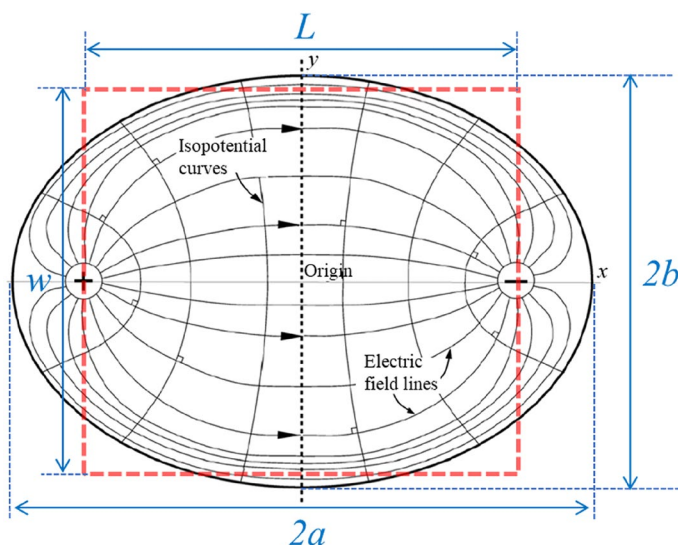
$$q = -\frac{k}{\mu}\nabla p, \tag{1}$$

where q is the fluid flux, i.e., volumetric flow rate per unit area [m/s], k is the permeability [m²], μ is the dynamic viscosity of fluid [Pa·s], ∇p is the fluid pressure drop over a given distance [Pa/m].

We made use of the optimization module in the COMSOL multi-physics software to estimate the hydraulic transmissivity through minimizing the relative error between the volumetric flow rates in the numerical model and the laboratory test using the Nelder–Mead method. Specifically, we considered a uniform fracture with an average effective thickness of t [m], and thus the volumetric flow rate Q [m³/s] in the numerical model is the product of the thickness t and the line integral of fluid flux q along the circumference of the inlet borehole. Thus, the constraint of the optimization can be mathematically described as:

$$\left| \frac{\oint qt}{Q_{exp}} - 1 \right| \le 0.01\%, \tag{2}$$

where Q_{exp} [m³/s] is the volumetric flow rate recorded in the laboratory. We input the volumetric flow rate, inlet and outlet pressures recorded in the laboratory into the numerical model and the hydraulic transmissivity can be obtained directly through optimization. Fig. 2a (right) demonstrates the steady state fluid pressure profile in the fracture with an inlet pressure of 8 MPa and an outlet pressure of 5 MPa, i.e., the first steady state flow measurement data point in Ye and Ghassemi (2018). The grey lines with arrows are the flow lines. The numerical back-calculation process of fracture transmissivity using the COMSOL multi-physics software is summarized in Fig. 2b.

3.2 Electrical Analogy

The electrical analogy relates the hydraulic and electrical conductivity of rock fractures, which has been used to derive the analytical solution for the transmissivity of an elliptical rock fracture. The flow lines between the inlet and outlet boreholes in Fig. 2a are analogous to the electric field lines between two electrodes in Fig. 3. For an elliptical rock fracture, the lengths in the slip-parallel and slip-normal directions are respectively 2*a* [mm] and 2*b* [mm], and the ratio *b/a* is defined as *n* (Fig. 3). For convenience, the source and sink holes (i.e., inlet and outlet boreholes) are assumed to lie on the elliptical boundary. The analytical solution for the transmissivity based on the electrical analogy is (Rutter and Mecklenburgh 2017, 2018):

$$(kt)_E = \frac{Q\mu}{\Delta p} \frac{\ln\left(\frac{2a}{r} - 1\right)}{B\pi}, \tag{3}$$

where Q is the volumetric flow rate [m³/s], Δp is the pressure difference between the inlet and outlet boreholes [Pa], r is the borehole radius, B is the geometry constant equal to *2/πarctan(2n)*. It may be noted that the equation that follows Eq. A1 in Rutter and Mecklenburgh (2018) contains an error, in which the pressure *gradient* is mistakenly shown instead of pressure *difference*.

3.3 Rectangular Approximation

For the fluid flow in a fracture, the hydraulic transmissivity can be derived from the integral form of Darcy's law (Eq. 1) as:

$$kt = \frac{Q\mu L}{w\Delta p}, \tag{4}$$

where w is the fracture width [m], L is the length along the flow direction [m].

To estimate the transmissivity of a rock fracture using Eq. 4, the fracture width w should be maintained constant along the flow path. In such case, the fluid is injected as a line source along the fracture width w, and similarly withdrawn over a line sink of the same width. However, in the case of an elliptical rock fracture, the fracture width w changes along the flow direction and the fluid is injected and withdrawn via a hole of negligibly small radius compared to other physical dimensions. Hence, for this case, a rectangular approximation was proposed by Ye and Ghassemi (2018), in which the flow region was assumed to be a rectangle with the same area as the elliptical rock fracture and with a length equal to the distance between the inlet and outlet boreholes (i.e., $L=2a$) (Fig. 3). The fracture width w can thus be calculated from the length of axis normal to the flow direction $2b$ [m] as $w=\pi b/2$ if once again the boreholes are assumed on the boundary. Thus, the transmissivity of the elliptical fracture that is estimated based on the rectangular approximation can be expressed as:

Fig. 4 Comparison of methods. **a** Hydraulic transmissivity (kt) obtained from the numerical back-calculation (N) as a function of that from the electrical analogy (E) using the experimental data of Ye and Ghassemi (2018). The 1:1 correlation between the results of the two approaches demonstrates their agreement. **b** Ratio of hydraulic transmissivity (kt) obtained from the rectangular approximation (R) and the electrical analogy (E) as a function of inclination angle with respect to the sample axis in the favorable angle range (Eq. 6). The two directions are indicated in the insets

(a)

(b)
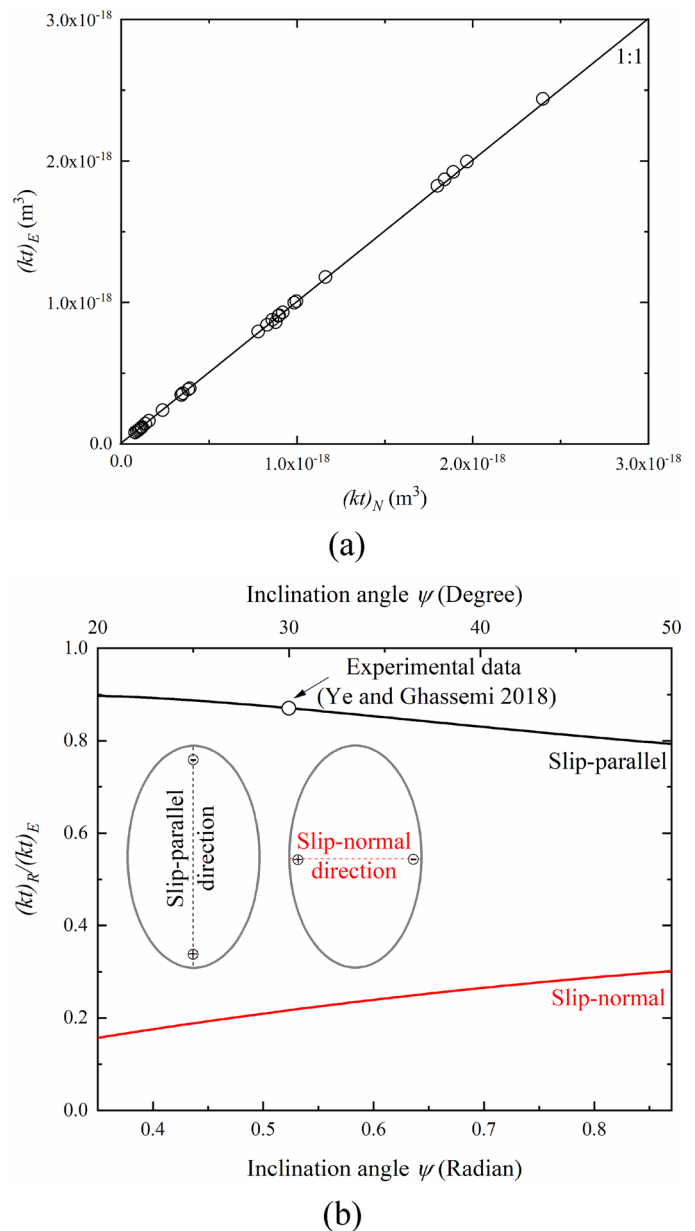
$$(kt)_R = \frac{4Qa\mu}{\pi b \Delta p}. \tag{5}$$

4 Comparison of Methods

Fig. 4a shows that the transmissivity obtained from the solution based on the electrical analogy is almost identical to that from the numerical back-calculation. The experimental data used here were collected from Ye and Ghassemi (2018). It, therefore, presents the simplest route to the accurate determination of hydraulic transmissivity from flow measurements through an elliptically shaped fracture.

We have shown above that our numerical model and the electrical analogy can both yield accurate transmissivity of elliptical rock fractures with a large JRC range, indicating that the accuracy of these two methods is nearly independent of the fracture surface roughness. The ratio between the transmissivity obtained from the rectangular approximation (Eq. 5) and the electrical analogy (Eq. 3) can indicate the accuracy of the rectangular approximation. Here, we extended it to include the effect of changing fracture inclination angle in both slip-parallel and slip-normal directions. The ratio is expressed as:

$$\frac{(kt)_R}{(kt)_E} = \frac{8 \arctan(2n)}{n\pi \ln\left(\frac{2a}{r} - 1\right)}, \tag{6}$$

where $n = sin\Psi$ and $2a = D/sin\Psi$ along the slip-parallel direction, while in the slip-normal direction, $n = 1/sin\Psi$, $2a = D$, where D is the sample end diameter.

Fig. 4b shows that when the inclination angle ranges from 20° to 50°, the transmissivity ratio in the slip-parallel direction reduces from 0.89 to 0.79, suggesting that the accuracy of the rectangular approximation is acceptable with an order-of-magnitude-accuracy. The experimental data of Ye and Ghassemi (2018) with an inclination angle of 30° show a transmissivity ratio in the slip-parallel direction of 0.87, consistent with the value predicted by Eq. 6. However, the transmissivity ratio in the slip-normal direction increases from 0.16 to 0.30 with increasing inclination angle from 20° to 50°, which means the rectangular approximation leads to a transmissivity approximately 1/4 of the true value. The transmissivity ratio $(kt)_R/(kt)_E$ in both directions decreases with larger n (i.e., the ratio between the lengths normal and parallel to the flow direction, $n = b/a$), consistent with the fact that the approximation of a point pressure source using a linear pressure source becomes more valid with increasing length parallel to the flow direction relative to the dimension normal to the flow direction. Moreover, the difference between the slip-normal transmissivity and the true value is always much larger than the slip-parallel transmissivity. This is also because the n value in the case of slip-normal transmissivity is always larger than the case of slip-parallel transmissivity.

5 Conclusions

We revisited the evaluation of the hydraulic transmissivity of elliptical rock fractures in triaxial shear-flow experiments. A COMSOL numerical model was constructed to obtain the transmissivity of elliptical rock fractures based on laboratory data. We estimated the transmissivity of fractures with JRC values ranging from 1.19 to 15.32 in a series of triaxial shear-flow experiments using the numerical back-calculation method, the electrical analogy and rectangular approximation. We compared the fracture transmissivity obtained from the three methods and concluded the following:

1. The transmissivity obtained from our numerical model and the electrical analogy are identical and represent the true transmissivity value. The rectangular approximation leads to a slightly underestimated slip-parallel transmissivity (0.79–0.89 times the true value) and a substantially underestimated slip-normal transmissivity (0.16–0.30 times the true value).
2. The underestimation of fracture transmissivity using the rectangular approximation is mainly attributable to the unmodified use of a point pressure source instead of a correct linear pressure source in the approximation.
3. Our study suggests that both the numerical back-calculation and the electrical analogy can be used for the accurate transmissivity determination of elliptical rock fractures, regardless of the fracture surface roughness. However, the rectangular approximation only provides a rough estimation of the slip-parallel transmissivity to an order-of-magnitude-accuracy.

References

Acosta M, Maye R, Violay M (2020) Hydraulic transport through calcite bearing faults with customized roughness: effects of normal and shear loading. J Geophys Res Solid Earth 125(8):e2020JB019767

Barton N (1973) Review of a new shear-strength criterion for rock joints. Eng Geol 7(4):287–332

Bernabé Y, Mok U, Evans B (2006) A note on the oscillating flow method for measuring rock permeability. Int J Rock Mech Min Sci 43(2):311–316

Bijay KC, Ghazanfari E (2021) Geothermal reservoir stimulation through hydro-shearing: an experimental study under conditions close to enhanced geothermal systems. Geothermics 96:102200

Bossart P, Meier PM, Moeri A, Trick T, Mayor J-C (2002) Geological and hydraulic characterisation of the excavation disturbed zone in the Opalinus Clay of the Mont Terri Rock Laboratory. Eng Geol 66(1):19–38

Brace W, Walsh J, Frangos W (1968) Permeability of granite under high pressure. J Geophys Res 73(6):2225–2236

Brady BH, Brown ET (1993) Rock mechanics for underground mining. Springer Science & Business Media

Byerlee JD (1967) Frictional characteristics of granite under high confining pressure. J Geophys Res 72(14):3639–3648

Crawford BR, Faulkner DR, Rutter EH (2008) Strength, porosity, and permeability development during hydrostatic and shear loading of synthetic quartz-clay fault gouge. J Geophys Res 113(B3)

Ellsworth WL (2013) Injection-induced earthquakes. Science 341(6142):1225942

Fang Y, Elsworth D, Wang C, Ishibashi T, Fitts JP (2017) Frictional stability-permeability relationships for fractures in shales. J Geophys Res Solid Earth 122(3):1760–1776

Faulkner DR, Rutter EH (2000) Comparisons of water and argon permeability in natural clay-bearing fault gouge under high pressure at 20°C. J Geophys Res Solid Earth 105(B7):16415–16426

Fischer GJ (1992) The determination of permeability and storage capacity: pore pressure oscillation method. In: Evans B, Wong T-F (eds) Fault mechanics and transport properties of rocks. Academic Press, New York, pp 187–212

Im K, Elsworth D, Fang Y (2018) The influence of pre-slip sealing on the permeability evolution on fractures and faults. Geophys Res Lett 45

Jeppson TN, Lockner D, Kilgore B, Beeler N, Taron J. Strength recovery and sealing under hydrothermal conditions. In: 55th US Rock Mechanics/Geomechanics Symposium 2021 Jun 18. Texas

Ji Y, Wu W (2020) Injection-driven fracture instability in granite: mechanism and implications. Tectonophysics 791:228572

Ji Y, Wu W, Zhao Z (2019) Unloading-induced rock fracture activation and maximum seismic moment prediction. Eng Geol 262:105352

Ji Y, Wanniarachchi WAM, Wu W (2020) Effect of fluid pressure heterogeneity on injection-induced fracture activation. Comput Geotech 123:103589

Ji Y, Fang Z, Wu W (2021) Fluid overpressurization of rock fractures: experimental investigation and analytical modeling. Rock Mech Rock Eng 54(6):3039–3050

Ji Y, Hofmann H, Duan K, Zang A (2022) Laboratory experiments on fault behavior towards better understanding of injection-induced seismicity in geoenergy systems. Earth-Sci Rev 226:103916

Ji Y (2020) Shear-flow characteristics of rock fractures and implications for injection-induced seismicity. Ph.D. thesis, Nanyang Technological University, Singapore

Kranz R, Saltzman J, Blacic J. (1990). Hydraulic diffusivity measurements on laboratory rock samples using an oscillating pore pressure method. In: Paper presented at the International Journal of Rock Mechanics and Mining Sciences and Geomechanics Abstracts.

Li Q, Ito K, Wu Z, Lowry CS, Loheide S II (2009) COMSOL multiphysics: a novel approach to ground water modeling. Groundwater 47(4):480–487

LongJohn T, Morgan JK, Dugan B (2018) Microstructural evolution of porosity and stress during the formation of brittle shear fractures: a discrete element model study. J Geophys Res Solid Earth 123(3):2228–2245

Ma X, Zoback MD (2017) Laboratory experiments simulating poroelastic stress changes associated with depletion and injection in low-porosity sedimentary rocks. J Geophys Res Solid Earth 122(4):2478–2503

Marone C, Scholz C (1989) Particle-size distribution and microstructures within simulated fault gouge. J Struct Geol 11(7):799–814

Milsch H, Hofmann H, Blöcher G (2016) An experimental and numerical evaluation of continuous fracture permeability measurements during effective pressure cycles. Int J Rock Mech Min Sci 89:109–115

Okazaki K, Katayama I, Noda H (2013) Shear-induced permeability anisotropy of simulated serpentinite gouge produced by triaxial deformation experiments. Geophys Res Lett 40(7):1290–1294

Passelègue FX, Brantut N, Mitchell TM (2018) Fault reactivation by fluid injection: Controls from stress state and injection rate. Geophys Res Lett 45(23):12837–812846

Passelègue FX, Almakari M, Dublanchet P, Barras F, Fortin J, Violay M (2020) Initial effective stress controls the nature of earthquakes. Nat Commun 11(1):5132

Rutter E, Hackston A (2017) On the effective stress law for rock-on-rock frictional sliding, and fault slip triggered by means of fluid injection. Philos Trans A Math Phys Eng Sci 375(2103):20160001

Rutter EH, Mecklenburgh J (2017) Hydraulic conductivity of bedding-parallel cracks in shale as a function of shear and normal stress. Geol Soc Lond Spec Publ 454(1):67–84

Rutter EH, Mecklenburgh J (2018) Influence of normal and shear stress on the hydraulic transmissivity of thin cracks in a tight quartz sandstone, a granite, and a shale. J Geophys Res Solid Earth 123(2):1262–1285

Scheidegger AE (1958) The physics of flow through porous media. Soil Sci 86(6):355

Shapiro SA, Huenges E, Borm G (1997) Estimating the crust permeability from fluid-injection-induced seismic emission at the KTB site. Geophys J Int 131(2):F15–F18

Shen H, Zhang Q, Li Q, Li X, Shi L, Shen N (2020) Experimental and numerical investigations of the dynamic permeability evolution of a fracture in granite during shearing under different normal stress conditions. Rock Mech Rock Eng 53(10):4429–4447

Shovkun I, Espinoza DN (2017) Coupled fluid flow-geomechanics simulation in stress-sensitive coal and shale reservoirs: Impact of desorption-induced stresses, shear failure, and fines migration. Fuel 195:260–272

Sibson RH (1990) Rupture nucleation on unfavorably oriented faults. Bull Seismol Soc Am 80(6A):1580–1604

Tembe S, Lockner DA, Wong T-F (2010) Effect of clay content and mineralogy on frictional sliding behavior of simulated gouges: Binary and ternary mixtures of quartz, illite, and montmorillonite. J Geophys Res 115(B3)

Wang X, Gao Q, Li X, Liu D, Wang Y (2021) Laboratory study on the effect of fluid pressurization rate on fracture instability. Geofluids 2021:1–8

Wang L, Kwiatek G, Rybacki E, Bonnelye A, Bohnhoff M, Dresen G (2020) Laboratory study on fluid-induced fault slip behavior: The role of fluid pressurization rate. Geophys Res Lett 47:e2019GL086627

Wanniarachchi WAM, Ranjith PG, Perera MSA, Rathnaweera TD, Zhang C, Zhang DC (2018) An integrated approach to simulate fracture permeability and flow characteristics using regenerated rock fracture from 3-D scanning: a numerical study. J Nat Gas Sci Eng 53:249–262

Ye Z, Ghassemi A (2018) Injection-induced shear slip and permeability enhancement in granite fractures. J Geophys Res Solid Earth 123(10):9009–9032

Zoback MD (2010) Reservoir geomechanics. Cambridge University Press, Cambridge